Linking the Transcriptional Landscape of Bone Induction to Biomaterial Design Parameters

Linking the Transcriptional Landscape of Bone Induction to Biomaterial Design Parameters

*Nathalie Groen, Huipin Yuan, Dennie G. A. J. Hebels, Gülistan Koçer, Faustin Mbuyi, Vanessa LaPointe, Roman Truckenmüller, Clemens A. van Blitterswijk, Pamela Habibović, and Jan de Boer**

New engineering possibilities allow biomaterials to serve as active orchestrators of the molecular and cellular events of tissue regeneration. Here, the molecular control of tissue regeneration for calcium phosphate (CaP)-based materials is established by defining the parameters critical for tissue induction and those are linked to the molecular circuitry controlling cell physiology. The material properties (microporosity, ion composition, protein adsorption) of a set of synthesized osteoinductive and noninductive CaP ceramics are parameterized and these properties are correlated to a transcriptomics profile of osteogenic cells grown on the materials in vitro. Using these data, a genetic network controlling biomaterial-induced bone formation is built. By isolating the complex material properties into single-parameter test conditions, it is verified that a subset of these genes is indeed controlled by surface topography and ions released from the ceramics, respectively. The gene network points to a decisive role for extracellular matrix deposition in osteoinduction by genes such as tenascin C and hyaluronic acid synthase 2, which are controlled by calcium and phosphate ions as well as surface topography. This work provides insight into the biomaterial composition and material engineering aspects of bone void filling and can be used as a strategy to explore the interface between biomaterials and tissue regeneration.

1. Introduction

The field of pharmacology has seen tremendous advances in the past decades after its adoption of high-throughput screening, the large-scale use of transcriptomics to decipher the biological complexity of diseases and their treatments, along with computational approaches to model the relationship between molecular structure and bioactivity. Although we and others heralded the promise of "materiomics," which refers to similar approaches for biomaterials,[1–4] the field is only slowly adopting these tools. This lag is partly explained by the high level of design complexity that biomaterial engineers face. Whereas most pharmaceutically active compounds act on single molecules (typically proteins), successful biomaterials also act at the cellular and tissue level. For example, a vascular stent opens the occluded blood vessel and facilitates endothelial and vascular smooth muscle cell adhesion, and titanium hip implants bond to bone at the cellular level while providing mechanical support to the bone as a whole. Materials ultimately interact at the molecular, cellular and tissue levels, and their effective design must consider this hierarchy.[5–10]

The use of animal models has been effective to study biomaterials at the tissue level, but understanding at the molecular and cellular levels has been impeded by the complexity of multiscale material properties that combine and converge to influence cell behavior.[11] For example, surface energy and wetting properties can affect protein binding and the subsequent adhesion of cells,[12] while surface topography and elasticity both affect mechanobiology.[13,14] While osteoblasts are essential for bone formation, macrophages and osteoclasts have also been suggested to play an important role.[15] Despite a number of high-quality studies that aim to improve our understanding of how material properties influence cell behavior, the relationship between the two is still a black box.[16–20]

In this study, we introduce a holistic approach toward understanding cell–biomaterial interactions by generating a transcriptional landscape of osteogenic cells coupled to parameters known to influence bone formation in vivo. We leveraged existing knowledge on calcium phosphate ceramics, which are widely applied as synthetic bone-graft substitutes, and have tunable parameters (e.g., crystallinity, porosity, chemical composition) that elicit profoundly different biological responses.[21] For instance, surface microstructure correlates to the induction of ectopic bone tissue in vivo.[22–24] Furthermore, calcium ions can induce the expression of the bone growth factor BMP2,[25–27]

Dr. N. Groen, G. Koçer, F. Mbuyi, Prof. J. de Boer
Department of Tissue Regeneration
University of Twente
Drienerlolaan 5, 7522 NB, Enschede, The Netherlands
E-mail: jan.deboer@maastrichtuniversity.nl
Prof. H. Yuan, Dr. D. G. A. J. Hebels, V. LaPointe, Dr. R. Truckenmüller, Prof. C. A. van Blitterswijk, Prof. P. Habibović, Prof. J. de Boer
MERLN Institute for Technology-inspired Regenerative Medicine
Maastricht University
Universiteitssingel 40, 6229 ER, Maastricht, The Netherlands
Prof. H. Yuan
Xpand Biotechnology B.V
Professor Bronkhorstlaan 10, 3723 MB, Bilthoven, The Netherlands

DOI: 10.1002/adma.201603259

and surface topography induced osteogenic differentiation,[28] but it is unknown if these parameters contribute to bone formation in vivo. In addition, the molecular mechanisms driving bone formation remain unclear, as are the material parameters that are causally linked to it. In this study, we define the material-induced transcriptional landscape in osteoblasts in vitro and show a correlation between in vivo bone formation and induction of a specific gene set by defined biomaterial parameters.

2. Results

2.1. Calcium Phosphate Synthesis Parameters Correlate to In Vivo Osteogenic Potential

In order to determine how material parameters correlate to their osteogenic potential, we produced a series of materials with three different chemical compositions: hydroxyapatite (HA); β-tricalcium phosphate (TCP); and a mixture of 80 ± 5% HA and 20 ± 5% β-TCP, referred to as biphasic calcium phosphate (BCP). Next, we varied the microstructural properties while preserving the chemical composition and macroporosity (**Figure 1**) by sintering the ceramics at different temperatures.

For both HA and BCP, we synthesized a material with relatively small grain size, high microporosity, and high specific surface area (named HAi and BCPi from here on) as compared to their counterparts (named HAn and BCPn from here on, Figure S1, Supporting Information) (the "i" and "n" stand for the osteoinductive and non-osteoinductive properties of these materials, respectively, as shown in the in vivo study at the end of this section). TCP particles (only one type) were prepared with structural properties similar to HAi and BCPi (Figure 1 and Figure S1, Supporting Information). To parameterize material

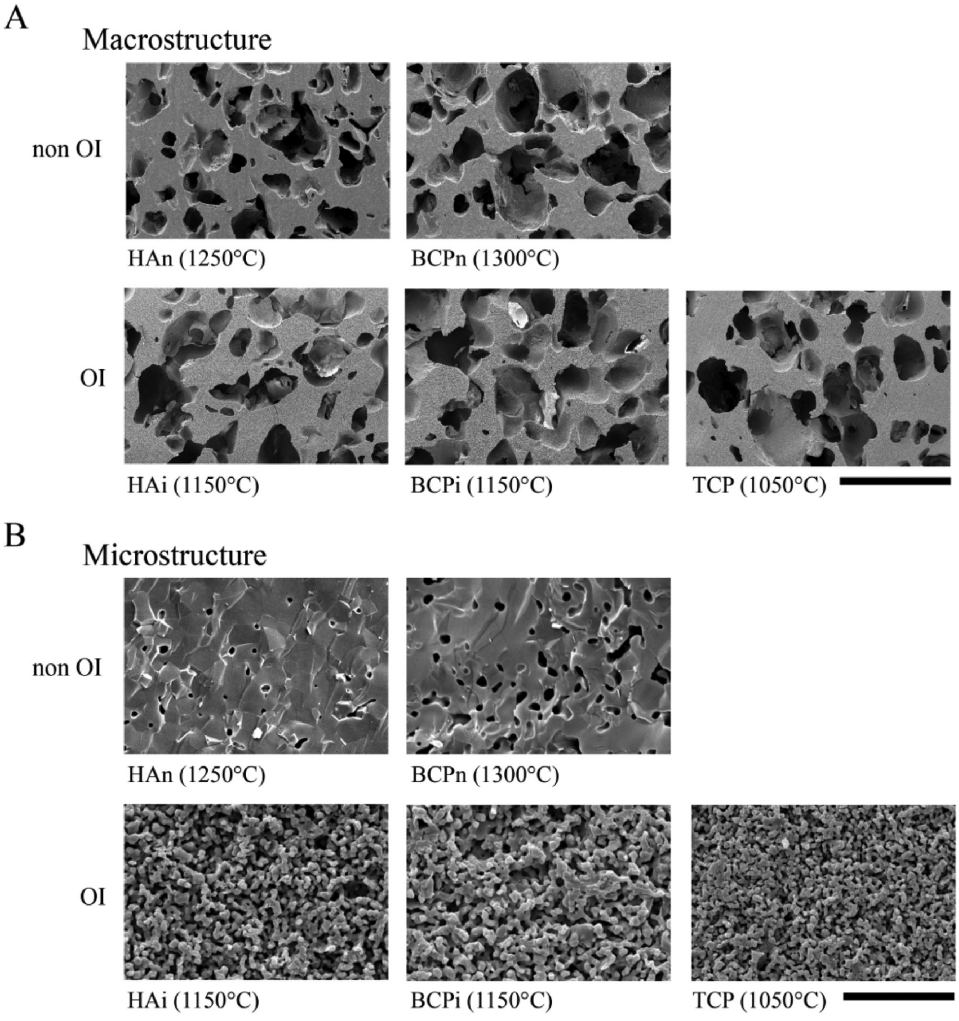

Figure 1. Macro- and microstructure of calcium phosphate ceramics. A) The macrostructure of the different ceramics sintered at varying temperatures is similar, as shown by SEM images of the polished ceramic bodies used to prepare the ceramic particles. A separation between non-osteoinductive (non OI; top row) and osteoinductive (OI; bottom row) ceramics is made, referring to the results of the in vivo osteoinductivity study (Figure S4, Supporting Information). B) In contrast, the microstructure of the non-osteoinductive ceramics (top row) is different from that of the osteoinductive ceramics (bottom row), as depicted by the SEM images. HA, hydroxyapatite; BCP, biphasic calcium phosphate; TCP, tricalcium phosphate particles, "i", osteoinductive; "n", non-osteoinductive (macrostructure scale bar is 1000 μm; microstructure scale bar is 20 μm).

properties, we measured porosity (Figure S1, Supporting Information), chemical composition, protein adsorption and calcium release, confirming that the material pairs differing in microstructure (BCPn–BCPi and HAn–HAi, respectively) had the same chemistry (Figure S2, Supporting Information). Protein adsorption was quantified after immersion in medium containing fetal bovine serum. Interestingly, the materials with unstructured surfaces (HAn and BCPn) adsorbed more protein relative to surface area than their microstructured equivalents and TCP (Figure S3, Supporting Information). In an earlier study by Wang et al.[29] comparing two different HA ceramics, a somewhat lower adsorption of rat serum was observed than in our study. In another study by Wang et al.,[30] comparing HA, BCP, and TCP ceramics, the total amount of proteins adsorbed on the ceramics were significantly lower than in our study. However, comparable to our findings, the ceramics with a lower specific surface area showed the highest adsorption of human serum protein. In contrast, in a study by Li et al.,[31] an opposite trend was observed for two BCP ceramics. It should be noted that these comparisons among different studies should be critically reviewed because of differences in experimental setup and the way data are presented. Nevertheless, they all suggest that both the structural and the chemical properties play a role in protein adsorption.

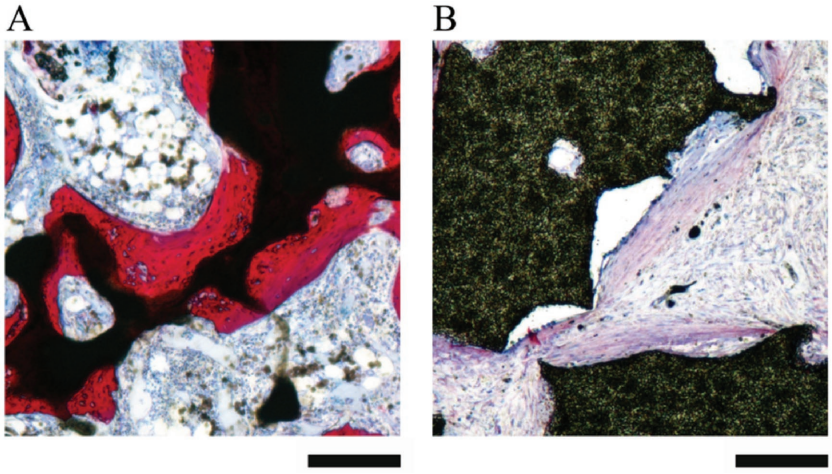

Figure 2. Induction of ectopic bone formation by microporous calcium phosphate ceramics. Osteoinductive potential of calcium phosphate ceramics implanted intramuscularly in dogs, 12 weeks after implantation. Representative histological sections are shown of (A) an osteoinductive calcium phosphate ceramic (TCP, left) and (B) a non-osteoinductive one (BCPn, right). Histological sections of all materials can be found in the Figure S4 in the Supporting Information. Basic Fuchsin stains the newly formed bone red, methylene blue stains fibrous tissue blue, and the scaffold is shown in black (scale bar is 250 µm). Osteocytes can be seen embedded in the bone matrix, and bone marrow can be seen in the top left corner of the TCP sample. In contrast, only fibrous tissue can be observed in the non-inductive ceramics.

Calcium release over a period of two weeks was highest from TCP (Figure S3, Supporting Information). Although both BCP materials had a similar calcium release, the release from HAi was comparatively higher, and the release from HAn was the lowest among all materials. It should be noted that the medium used for the release study, the simulated physiological solution, represents the pH and the ionic strength of a physiological environment, but not the level of saturation with calcium and inorganic phosphate ions. In vivo, where body fluids contain approximately 2×10^{-3} M and 1×10^{-3} M calcium and phosphate, respectively, none of these ceramics is expected to be soluble. This was also supported by our earlier studies in which the concentrations of calcium and phosphate were measured upon immersion of the ceramics in alpha-MEM or cell culture medium.[32–34] In these studies, a decrease of calcium and inorganic phosphate concentrations was observed. Nevertheless, in our previous study in vivo we observed extensive degradation of TCP.[35] Indeed, within 12 weeks of implantation in bone, more than 50% of the implanted material was degraded, showing that also in vivo, calcium and phosphate release occurs.

Here, in order to assess their biological activity, we implanted the materials intramuscularly in dogs and examined ectopic bone formation after 12 weeks by histomorphometry. We observed a correlation between the structure of the materials and bone formation. In chemically paired compositions, the microstructured version of the materials induced ectopic bone formation whereas no bone was induced by the unstructured materials (**Figure 2** and Figure S4, Supporting Information).

In summary, we produced and defined the microstructural characteristics and bioactivity for five ceramic materials. In the next sections, we studied the cellular and molecular mechanisms of the material–cell interactions for these ceramic materials using transcriptomics. We focused in particular on the influence of structural and chemical material parameters.

2.2. Pathway Analysis and Genetic Network Creation for Osteoinductivity

Before zooming in on the role of specific material characteristics on the transcriptome of the cell, we first performed a more general analysis of transcriptomic differences, focusing on pathway and network analysis. To describe the genetic interactions related to in vivo osteoinductivity, we analyzed the transcriptomic response of the human MG-63 osteogenic cell line cultured on chemically identical material pairs (HAi vs HAn; BCPi vs BCPn) (**Figure 3**). The HA-based and BCP-based material comparisons respectively revealed 168 and 3247 genes to be differentially expressed. Eighty-eight genes overlapped between these two lists and these were used for further analysis (Table S1, Supporting Information). We performed a pathway over-representation analysis using the ConsensusPathDB tool (CPDB) to see if our overlap gene list is involved in any established signaling pathways. Three significantly overrepresented signal transduction pathways involving 10 significant genes were found: i) pharmacodynamics of vemurafenib, ii) HIF-1-alpha signaling, and iii) integrin cell surface interactions (**Table 1**). The top pathway describes the effect of vemurafenib, which is at first sight a

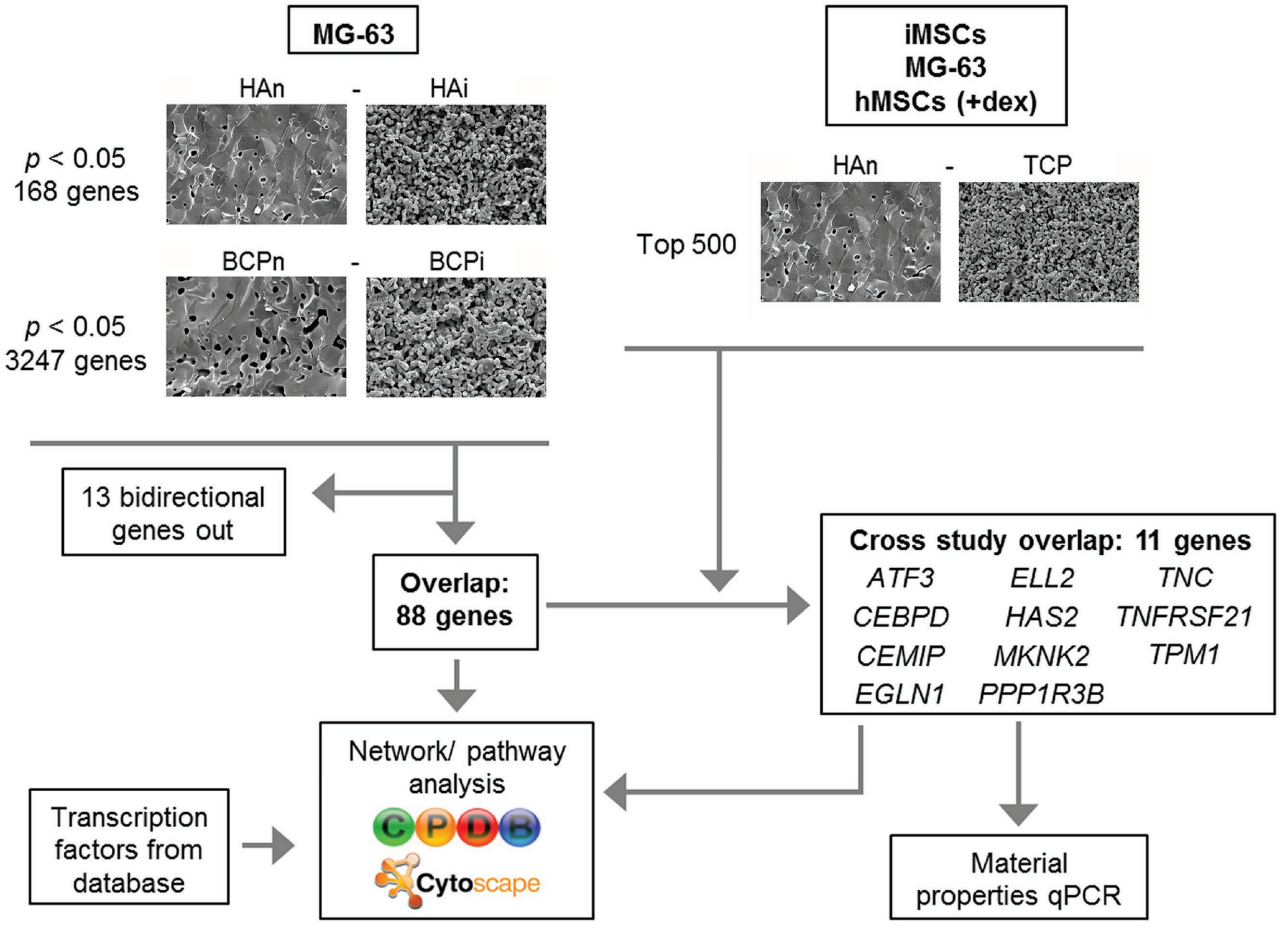

Figure 3. Gene selection and analysis procedure. Genes differentially expressed in MG-63 cells cultured on non-osteoinductive and osteoinductive materials (HA and BCP) were determined as described in the Methods section, and 88 genes overlapped between osteoinductive HA and BCP. The top 500 differentially expressed genes between non- and osteoinductive ceramic materials were compared in MG-63 (two independent microarray datasets), iMSCs, and hMSCs, then checked for overlap with our list of 88 genes. This comparison resulted in 11 cross-study overlapping genes.

confusing hit because vemurafenib is a compound used to treat metastatic melanoma. However, it is also known to have the side-effect of inhibiting osteogenesis, which explains why it shows up in this analysis.[36] This is not surprising because the genes that are affected in this vemurafenib-induced pathway (i.e., MAPK3, PDGFRA and ETS1) are all known to be key players in osteogenesis.[37,38] The HIF-1-alpha transcription factor pathway is hypoxia-responsive and plays a crucial role in developing bone by coordinating new blood vessel formation,[39] while integrin signaling has been shown to influence osteogenesis and osteoblast differentiation.[40] Indeed, our osteoinductivity overlap gene list is involved in highly relevant established signaling pathways.

Table 1. Significantly over-represented pathways found in CPDB.

Pathway	Source	Significant gene members[a)]	q-value[b)]
Vemurafenib Pathway, Pharmacodynamics	PharmGKB	MAPK3; PDGFRA; ETS1	0.0208
HIF-1-alpha transcription factor network	PID	HK2; CXCL12; ETS1; EGLN1	0.0208
Integrin cell surface interactions	Reactome	CD47; COL13A1; ITGB5; TNC	0.0208

[a)]As found in the list of 88 genes; [b)]The *q*-value represents the over-representation analysis *p*-value corrected for false discoveries.

We next used our overlap gene list to create a gene network in CPDB in order to visualize the interactions between the 88 osteoinduction genes and their co-regulated genes, enabling us to uncover relationships between corresponding proteins, intermediate signaling proteins, and crucial transcription factors. Since such networks are based on continuously updated databases, new connections can be discovered, not yet recorded in established pathways. Using the network analysis tool CytoScape, additional transcription factors and targets, derived from the ENCODE transcription factor database, were added to the network (Figure S5A, Supporting Information). Hub genes that play a central role in this osteoinductivity network were subsequently identified by determining the number of connections from each protein (Figure S5B, Supporting Information). Five genes with a very high connectedness were identified (*ATF3, BATF, ETS1, JUND, MAFF*), all transcription factors affecting up to several hundred target

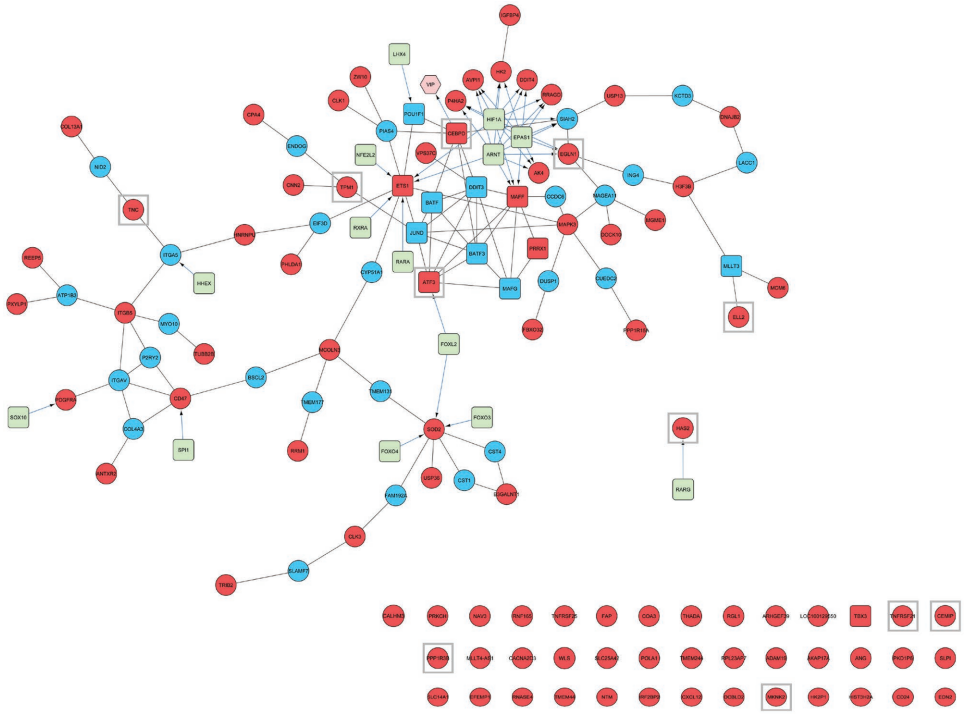

Figure 4. Network constructed through an initial network formation in CPDB followed by CyTargetLinker analysis in CytoScape using the TFe database. Original osteoinductivity-related input genes (48 connected + 40 unconnected), genes added by CPDB (33), and genes added by CyTargetLinker (14) are represented by filled red, blue, and green nodes, respectively. Transcription factors are indicated with rounded squares and non-transcription factors by circles (CPDB) or hexagons (CyTargetLinker). The positions of the 11 cross-study genes are indicated with gray boxes.

genes. *ATF3, ETS1,* and *MAFF* were also present in our list of 88 overlapping genes.

To condense the network to a visually more manageable size, we performed a second network analysis in CytoScape using the considerably smaller Transcription Factor Encyclopedia (TFe) database, which draws information solely from manually curated literature. **Figure 4** shows high connectedness and a long signaling cascade with 14 additional TFe transcription factors and 1 target gene (VIP). Interestingly, 9 out of 10 of the differentially expressed genes that were found in the significant pathways in Table 1 were also found in this network. The network represented in Figure 4 provides a map of the molecular mechanisms regulating osteoinduction. Interestingly, a dense cloud of correlated genes is seen around the hypoxia inducible factors 1 and 2 (HIF1A, EPAS1, ARNT), suggesting a role for hypoxia signaling in osteoinduction.

2.3. Four Genes As Basis for a Molecular Model of Osteoinduction

For the next step in our transcriptomics approach, we wanted to select a small set of genes to investigate in greater detail with respect to their relationship to specific material properties. Genes correlating to material-induced bone in vivo should ideally also be regulated in other osteogenic cell lines and by other known osteoinductive materials. Therefore, we examined the overlap between our data set and three previously published transcriptomics datasets in which three cell types (immortalized and primary bone marrow mesenchymal stem cells, and MG-63 cells) were cultured on osteoinductive versus non-inductive ceramic materials (TCP and HA).[32,41] Doing so enabled us to filter down to a smaller set of robust genes involved in osteoinductivity. Twelve genes (Figure 3, **Table 2**) overlapped between these data sets, of which seven are identified in our network, and six of which are in the main signaling cascade (Figure 4). To validate these seven genes independently, we performed an RT-PCR experiment in MG-63 cells on the osteoinductive versus non-inductive ceramics (HAn vs HAi; BCPn vs BCPi) (**Figure 5** and Figure S6, Supporting

Table 2. List of 11 cross-study overlap genes with their full name.

Official Symbol	Name
ATF3	Activating transcription factor 3
CEBPD	CCAAT/enhancer binding protein (C/EBP), delta
CEMIP	Cell migration inducing protein, hyaluronan binding
EGLN1	Egl-9 family hypoxia-inducible factor 1
ELL2	Elongation factor, RNA polymerase II, 2
HAS2	Hyaluronan synthase 2
MKNK2	MAP kinase interacting serine/threonine kinase 2
PPP1R3B	Protein phosphatase 1, regulatory subunit 3B
TNC	Tenascin C
TNFRSF21	Tumor necrosis factor receptor superfamily, member 21
TPM1	Tropomyosin 1 (alpha)

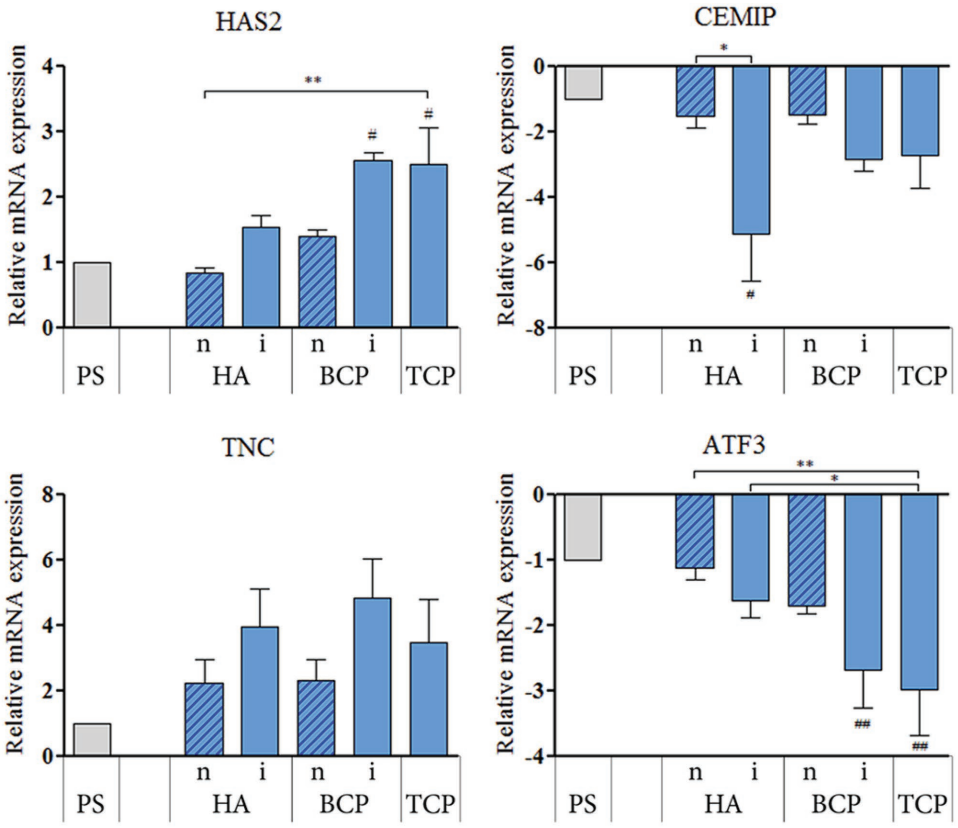

Figure 5. Gene expression validation. Relative mRNA levels (fold change) of the four core genes on non- and osteoinductive HA and BCP, as well as on osteoinductive TCP, versus tissue culture polystyrene (PS). The expression of *HAS2*, *CEMIP*, *TNC*, and *ATF3* was altered after 48 h of culture on the different ceramics (triplicate experiment). ANOVA with Bonferroni correction was used to test the statistical significance of the expression between the non- and osteoinductive ceramics (*$p < 0.05$, **$p < 0.01$). ANOVA with Dunnett correction was used to test the statistical significance (#$p < 0.05$, ##$p < 0.01$) of the differential expression between MG-63 cultured on the materials and PS.

Information). *HAS2, CEMIP, ATF3, TNFRSF21* and *TNC* were found to be differentially expressed. In addition, all but *TNFRSF21* were expressed higher on osteoinductive TCP ceramics than on the non-inductive HAn and BCPn. Interestingly, these four core genes (*HAS2, CEMIP, ATF3*, and *TNC*) all have a well-described role in the osteogenic process but have not as of yet been associated with biomaterial-induced bone formation. We also assessed the expression of *BMP2* (not a core gene), which responds to calcium and phosphate ions.[42] *BMP2* was significantly upregulated on the TCP particles compared to the unstructured HAn, BCPn, and polystyrene, but not between HAi and HAn (Figure S6, Supporting Information).

Having selected a list of robust core genes, in the next section we examined their role with respect to specific material properties. For this we used an approach where we deconvoluted material properties and linked this to gene expression levels based on RT-PCR.

2.4. Deconvolution of Material Properties

Ceramic materials are complex systems with highly intertwined material properties and concomitant biological effects. To further unravel the material property that caused the observed gene expression differences, we attempted to simplify the ceramic system by deconvoluting the material properties. We chose microstructure and ion release as two material properties involved in the osteogenic process based on our previous studies.[25,32,41] We engineered two experimental settings in which we could avoid confounding effects of other material parameters. To investigate the effect of topography on the expression of the four core genes, we produced a series of micro-roughened surfaces in polystyrene. To this end, we replicated the surfaces of two TCP-based ceramic discs with two different temperatures (1150 °C and 1050 °C for TCPa and TCPb, respectively) into polystyrene (termed PSa and PSb). We chose these disc-based ceramics because it is not possible to reproduce microstructures of particles, and because these discs induce bone formation in vivo with a clear relation between osteoinduction and micrometer-scale roughness (Figure S7, Supporting Information). Quantification of the grains on the imprinted surfaces revealed similar dimensions as the original ceramics (**Figure 6**). After confirming that the microstructured polystyrene surfaces allow cell adhesion and growth, gene expression of the four core genes was assessed after 7 days of MG-63 culture. The expression of *TNC, HAS2, CEMIP,* and *ATF3* was inversely related

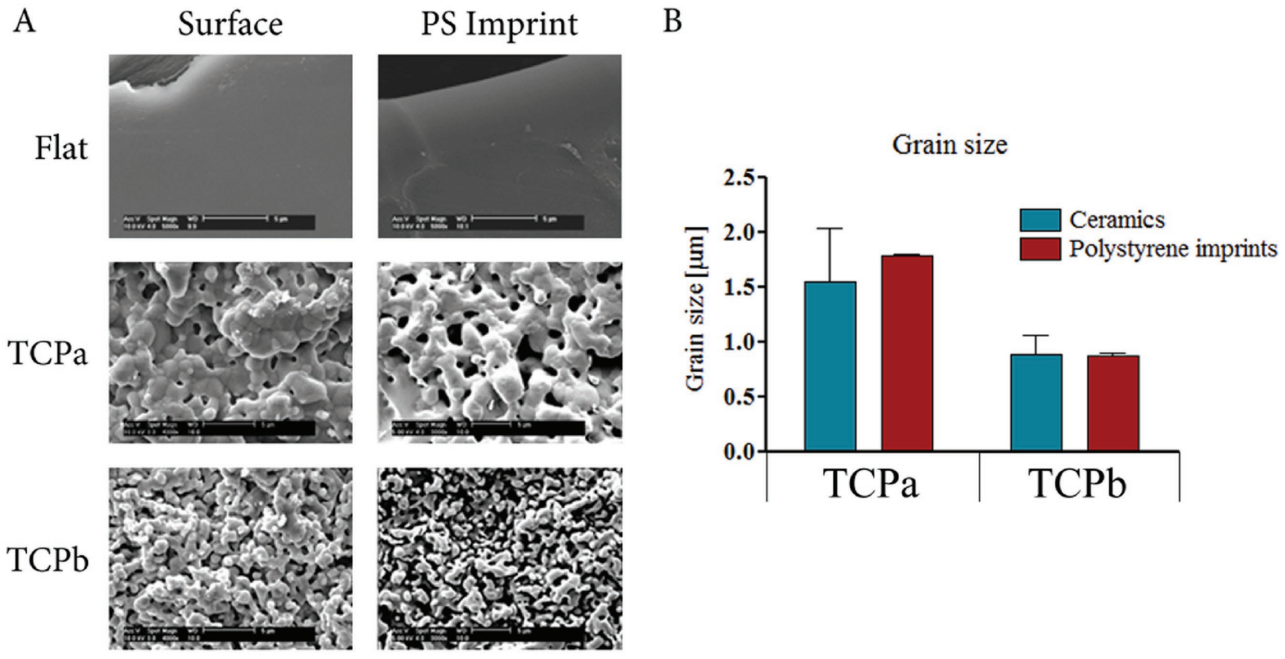

Figure 6. Replication of ceramic surfaces in polystyrene. A) The left column of images represents the surfaces of three TCP discs sintered at varying temperatures (1150 and 1050 °C; TCPa and TCPb, respectively) and a flat cyclic olyfinic polymer surface used as intermediate in the replication process. The right column of images depicts the surfaces in polystyrene (PS) replicated using micropatterning tools (scale bar is 5 µm). B) The grain sizes were measured on both the original ceramic surfaces and the imprinted PS surfaces to confirm replication of the surface structure. Average grain size was determined from 60 different grains from three independent SEM images using Image J. There are no significant differences between ceramics and PS imprints.

to grain size: mRNA levels for all four genes were greatest on the replicated surface of TCPb (PSb, **Figure 7**). *TNC* showed a significant, 4.5-fold upregulation on PSb compared to the flat surface. *BMP2* expression did not respond consistently to the surface of the imprints.

While topographical cues play a key role in cellular responses to ceramics and biomaterials in general, the presence of calcium and inorganic phosphate ions have also been shown to greatly affect cell behavior.[25,32] We therefore asked whether expression of the four core genes associated with osteoinductivity is influenced by these two ions. MG-63 cells were cultured in medium containing elevated levels of calcium (7.8×10^{-3} M) and phosphate (10×10^{-3} M) relative to basic medium (1.8×10^{-3} M calcium and 1×10^{-3} M phosphate, respectively). During these experiments no precipitation of calcium phosphate was observed. Of the four core genes, only *CEMIP* and *TNC* responded significantly to the ions (**Figure 8**). The expression of *CEMIP* significantly decreased in the presence of elevated calcium and phosphate levels in the culture medium. These two ions separately downregulated the expression by approximately 7-fold, whereas the combination of the two induced a 30-fold decrease after two days in culture. The effect on *TNC* was milder, with a 2- to 3-fold upregulation in the varying conditions, similar to the effect size observed on the different ceramics. Furthermore, a significant upregulation of *BMP2* (not a core gene) was observed when MG-63 cells were exposed to the combined high calcium and phosphate concentrations. In conclusion, *CEMIP* and *TNC* were significantly affected by the presence of calcium and/or inorganic phosphate ions.

2.5. A Potential Role for Hyaluronic Acid in Osteoinductivity

Of the four core genes, *HAS2* and *CEMIP* are both involved in hyaluronic acid synthesis, indicating a role for hyaluronic acid in ceramic-induced osteogenesis. To check whether differential expression of the genes correlated to different levels of hyaluronic acid, we quantified its presence in the extracellular matrix of MG-63 cells grown on ceramic particles. Indeed, hyaluronic acid was consistently produced more by cells on osteoinductive ceramics than non-inductive ceramics (**Figure 9**A). Moreover, we detected more of the biologically active high-molecular-weight chains (Figure 9B).

3. Discussion

What triggers osteogenic cells to form bone tissue in vivo? More specifically, which signals from biomaterials initiate this response and how do cells transmit them to execute the osteogenic program? This knowledge is essential to both rationally design and implement screening strategies to engineer bioactive materials.[8] To this end, we present the transcriptional landscape of biomaterial-induced bone formation in vivo and uncover a role for hyaluronic acid synthesis in the initial steps of osteoinduction. Furthermore, we identified biomaterial parameters that regulate gene expression, and provide a transcription factor network potentially involved in the regulation of material-induced bone formation. This report unravels part of the molecular mechanism behind ceramic-induced bone

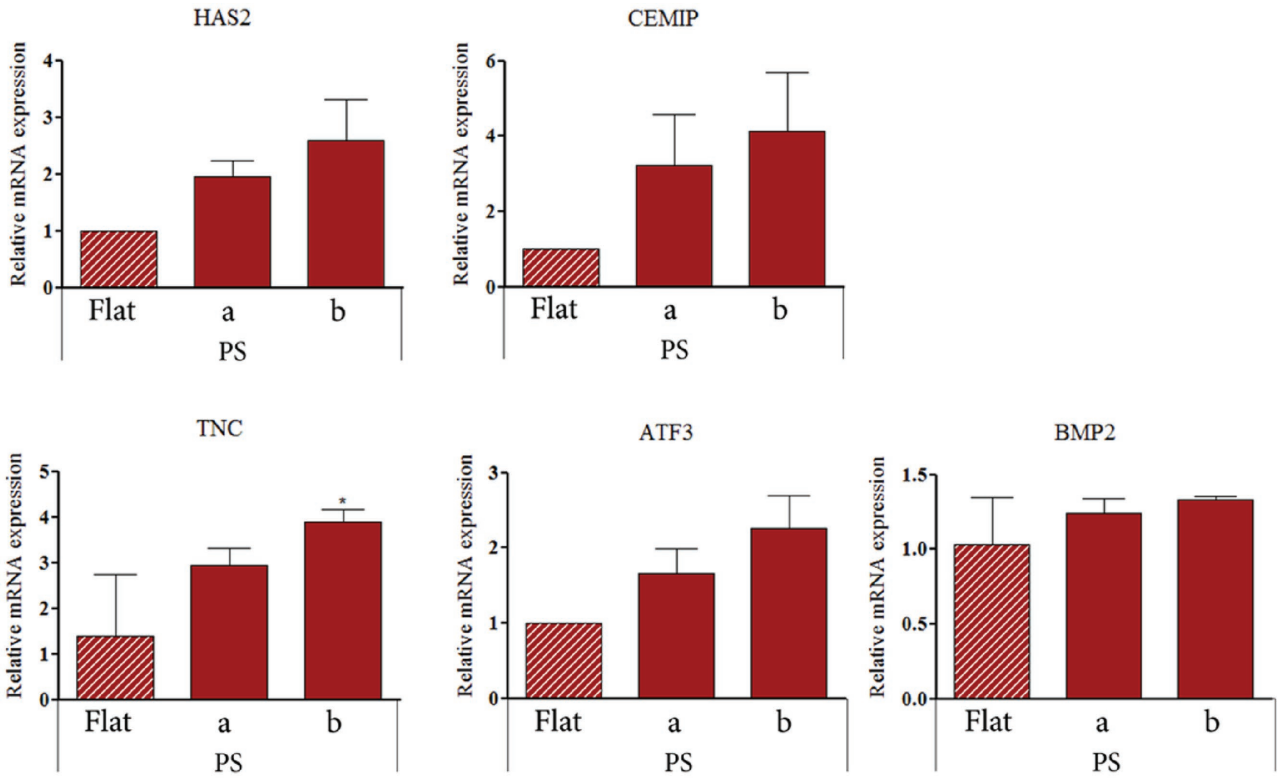

Figure 7. Gene expression on polystyrene mimicking ceramic surfaces. Relative mRNA levels (fold change) of *HAS2*, *CEMIP*, *TNC*, *ATF3* (core genes) and *BMP2* in MG-63 cells cultured on PSa and PSb (replicated from TCPa and TCPb respectively) versus flat PS (triplicate experiment) for 7 days. ANOVA with post-hoc Tukey was used to test statistical significance (*$p < 0.05$). Besides the indicated significance between PSb and flat for TNC, no statistical significance was reached in any of the other comparisons between flat, PSa, and PSb.

formation, which also represents a paradigm for analysis of tissue formation at the biomaterial interface in which both the complexity of biology and materials are parameterized and correlated (**Figure 10**).

Reverse engineering of osteoinduction in vivo has to deal with three levels of complexity: cells (cellular mechanisms), materials (topography and chemical interactions at the material surface), and tissues (multicellular environment including the extracellular matrix). In this study, we approach cellular complexity by using transcriptomics, in which the expression of all genes is assessed in vitro and correlated to bone formation in vivo. Analysis of our data revealed the involvement of previously identified osteogenic mechanisms such as integrin signaling[43] and the MAPK, ERK, AP-1 pathway.[44] We also found that the transcription factor HIF1α potentially acts as a hub protein regulating the expression of a significant number of genes in our network, analogous to its role in in vivo bone formation.[45] Studies investigating whether a causal link exists between hypoxia signaling and osteoinduction are in progress. Although the BMP signaling cascade did not emerge from our analysis, the role of hyaluronic acid synthesis and the confirmed induction of BMP2 on inductive ceramics does point to a role for BMP2. We hypothesize that osteoinductive ceramics trigger the osteoprogenitor to secrete an extracellular matrix rich in hyaluronic acid. Its known potentiating effect on the biological activity of BMP could thus provide part of the osteoinductive signal.[46] We are currently investigating whether a calcium/phosphate–hyaluronic acid–BMP2 axis plays a role in osteoinductivity. Hyaluronic acid is also known to interact with other growth factors, such as BMP7 and VEGF.[47,48] Whether this also plays a role in the calcium–phosphate–hyaluronic acid axis remains to be investigated.

In the studies reported here, focused parameters of material complexity were analyzed for their effect on specific gene expression. Although we were able to demonstrate that our four core genes responded to some combination of surface topography, calcium, and phosphate ions, how these three variables affect the expression of individual genes in our network remains to be determined. Moreover, we need to examine additional parameters, such as protein binding, of inductive ceramics. We observed that osteoinductive ceramics have a high amount of protein per volume of ceramic, but relatively low binding relative to the surface area. Additionally, future studies are needed to validate our gene network using other osteoinductive materials. For instance, we observed that 3D ceramic particles outperform their chemically identical discs in terms of bone induction in vivo, implicating a role for the macroporous architecture in the osteoinductive process,[49] for instance by tuning cell–cell interaction. Alternatively, the pores provide a chemically isolated niche in which both ions released from the materials and the molecules secreted by the osteogenic cells reach a critical level to boost osteogenesis. We therefore advocate the establishment of libraries of benchmark materials, in which material parameters are independently designed and

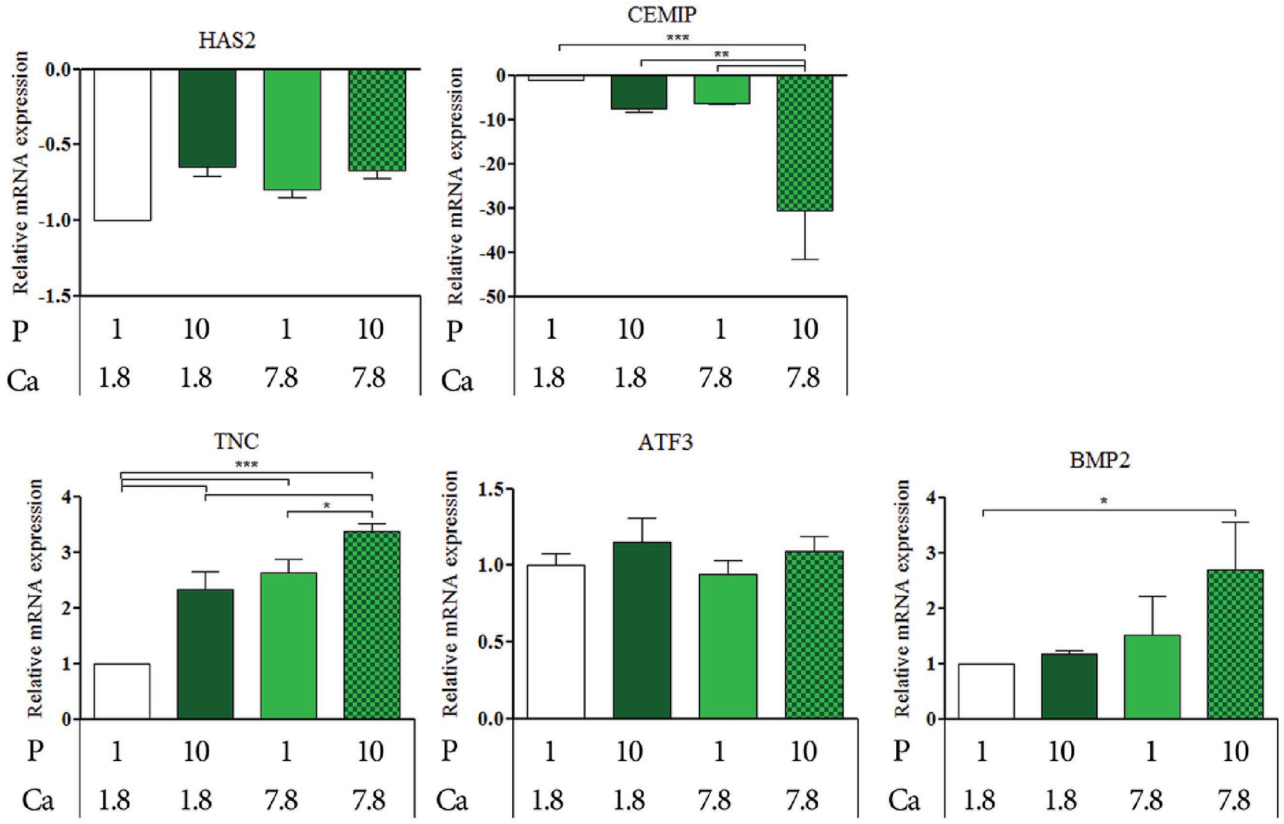

Figure 8. Gene expression under the influence of calcium or phosphate ions. MG-63 cells were cultured on polystyrene in the absence of ceramics in the presence of the respective ions (concentrations indicated in mM; triplicate experiment) for 48 hours. Relative mRNA levels (fold change) of *HAS2*, *CEMIP*, *TNC*, ATF3 (core genes), and *BMP2* versus basic medium (1.8×10^{-3} M Ca and 1×10^{-3} M phosphate; white bars) are shown. ANOVA was used to test statistical significance and only fold changes exceeding 2.5 were reported significant ($*p < 0.05$, $**p < 0.01$, $***p < 0.001$).

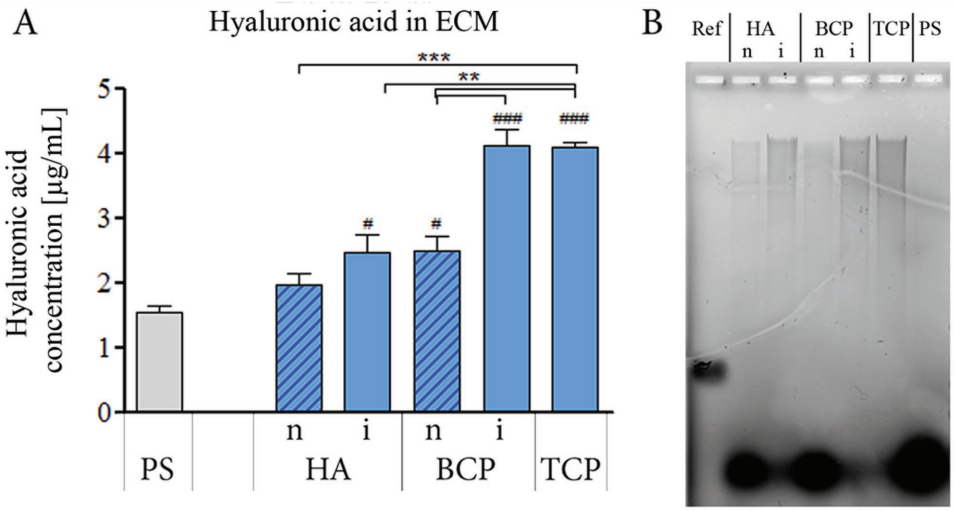

Figure 9. Hyaluronic acid production by MG-63 cultured on ceramics. A) Hyaluronic acid was extracted from the extracellular matrix (ECM) of MG-63 cultured on ceramics or flat polystyrene (PS) and quantified by ELISA in duplicate. ANOVA with Bonferroni correction was used to test the statistical significance between ceramics ($**p < 0.01$, $***p < 0.001$) or between ceramics and PS ($\#p < 0.05$, $\#\#\#p < 0.001$). B) Hyaluronic acid molecular-weight distribution by gel electrophoresis. The first gel lane contains a low-molecular-weight hyaluronic acid reference (15–30 kDa), whereas the higher-molecular-weight hyaluronic acid is mostly found in the ECM of MG-63 cells grown on osteoinductive CaP ceramic samples (HAi, BCPi, TCP), where it is present as a smear in the upper part of the lanes. The bands at the bottom consist of other low-molecular-weight glycosaminoglycans.

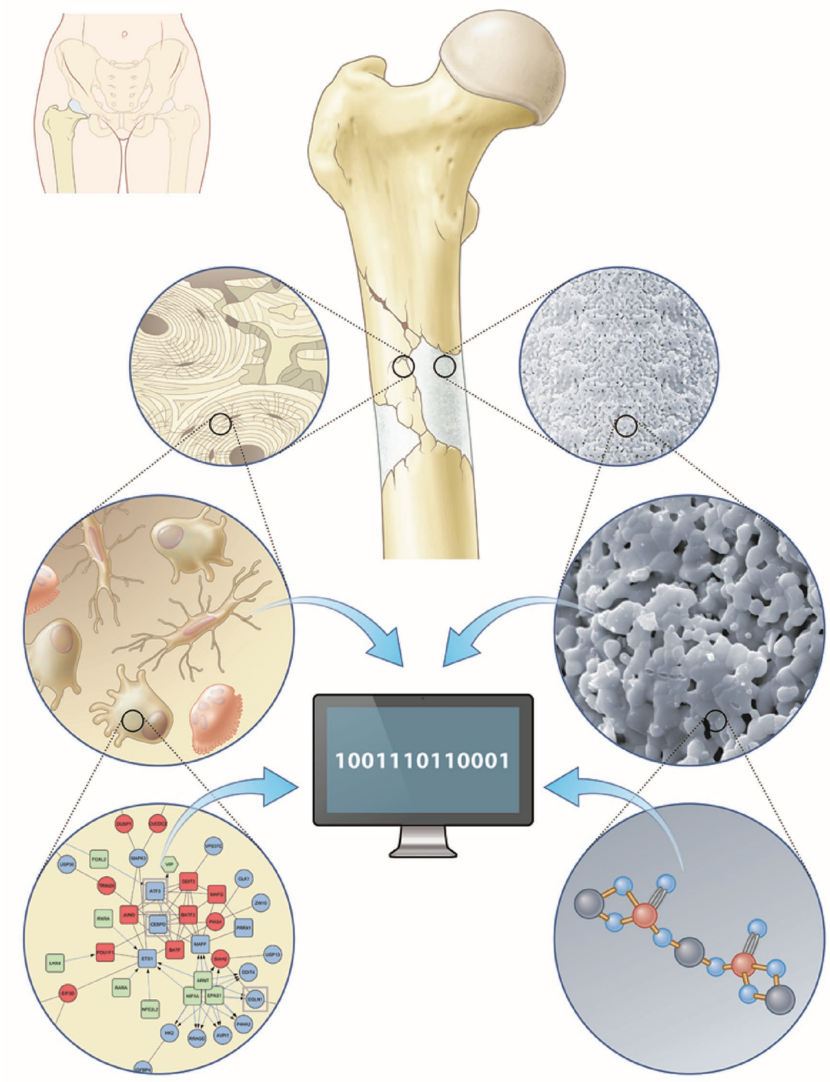

Figure 10. Integration of biology and material science toward a computational approach for new biomaterial development. Both bone (left) and bone-graft substitutes (right) can be deconstructed into their elementary components, i.e., gene expression and single material parameters, respectively. The interplay between them can be studied using computational approaches.

their effects on the osteogenic transcriptional landscape independently determined.

The final level of complexity of osteoinduction is the tissue. We chose to investigate the osteoblast cell line MG-63 because it is known to respond to many known osteogenic signals such as BMP2,[50] PTH, and vitamin D3.[51] Furthermore, we previously observed that inductive ceramics can induce ectopic bone formation by mesenchymal stem cells, which points at a bone-inducing effect at the level of the osteoprogenitor cell.[35] However, material-induced bone formation is a process that takes several weeks, during which the materials are sequentially interacting with a multitude of cell types ranging from pericytes to neutrophils, osteoclasts,[52] macrophages, and endothelial cells. Indeed, a role for macrophages in osteoinduction has been proposed[53] and it would be interesting to see how macrophage-derived signals feed into the molecular circuitry described in this paper. Eventually, the complexity of material-induced bone formation should be studied in vivo, for instance in the osteoinductive mouse model we recently discovered.[54] State of the art technologies such as tomo-sequencing[55] or in situ sequencing[56] may provide the spatiotemporal resolution needed to investigate the molecular events leading to bone formation.

4. Conclusions

We presented a transcriptional landscape of material-induced bone formation and were able to correlate expression of individual genes in this network to defined material parameters. The potential role of hyaluronic acid deposition by osteoprogenitors in the osteoinductive process is a starting point for unraveling the molecular mechanism and a biological readout for material engineering.

5. Experimental Section

5.1. Synthesis of Calcium Phosphate Ceramics

The materials in this study were used in three forms: macroporous particles (as used in Figure 1, 3, 5, and 9, and Figure S1–S3 and S6, Supporting Information), discs without macropores ("dense discs," as used in Figure 6), or cylinders with cut gaps ("dense cylinders," as used in Figure 2 and Figure S4 and S7, Supporting Information). For all forms, five different porous calcium phosphate ceramic bodies were prepared from apatite powders with Ca/P ratio of 1.67 (HA), 1.64 (BCP), or 1.50 (TCP). Briefly the apatite powders were either purchased (for HA, product number 1.02196.9025, Merck Millipore) or wet synthesized (for BCP and TCP) with calcium- and phosphate-containing solutions (calcium hydroxide, purum p.a., Fluka (product number C991T92) and phosphoric acid ≥85%, puriss. p.a. Ph.Eur, Sigma–Aldrich: Fluka (product number 79620), respectively), then green bodies were made with diluted H_2O_2 solution (1–2%) and wax particles at 60 °C. The green bodies were obtained after sintering at high temperatures for 8 h. The sintering temperatures were as follows: 1150 °C for HAi, 1250 °C for HAn, 1150 °C for BCPi, 1300 °C for BCPn, and 1050 °C for TCP. The particles (1–2 mm) were crushed, sieved, and ultrasonically cleaned with acetone, 70% ethanol and demineralized water, dried at 80 °C, and sterilized in an autoclave at 121 °C for 30 minutes. All chemicals were AR grade.

Next, dense green ceramic bodies were prepared from synthesized apatite powder with a Ca/P ratio of 1.50 using diluted H_2O_2 solution (0.1%) at ambient temperature and sintered at 1150 °C (TCPa) or 1050 °C (TCPb, similar to macroporous TCP particles described above). Dense ceramic discs (Ø 9 mm × 1 mm) and cylinders (Ø 9 mm × 10 mm) with two cut gaps (0.8 mm in width) were machined from the ceramic bodies using a lathe and a diamond-coated saw microtome, and were ultrasonically cleaned, and heat sterilized at 160 °C for 2 h. The gaps were created in order to allow for bone growth into the cylinder gap.

5.2. Material Characterization of the Calcium Phosphate Ceramics

The chemical properties and crystal structures of CaP ceramics were analyzed using Fourier transform infrared (FTIR) spectroscopy (Spectrum100, Perkin Elmer) and X-ray diffraction (XRD) (Miniflex, Rigaku, Japan).

The macro- and microstructure of the ceramics were imaged on polished ceramic bodies with a scanning electron microscope (SEM; XL30, Philips) in the secondary electron mode. The grain sizes of the ceramics were determined by measuring the lateral distance of 60 different grains from three independent SEM images using Image J. The pore size distribution, microporosity (volume percentage of pores smaller than 10 µm) and specific surface area were determined using mercury intrusion porosimetry (Quantachrome Instruments, Pore Master). Density measurements were performed to determine the true (skeletal) density of the materials using a helium pyconometer (Accu Pyc II 1340 gas pyconometer, Micrometrics) and analyzed with Pore Master software.

Calcium ion release profiles were determined by incubating 75 µL of ceramic granules in 1 mL of simulated physiological saline (SPS) (137×10^{-3} M Na^+, 177×10^{-3} M Cl^- and 50×10^{-3} M 4-(2-hydroxyethyl)-1-piperazineethanesulfonic acid (HEPES), pH 7.3 at 37 °C in demineralized water) with mild shaking (50 rpm) in a water bath and subsequently measuring calcium content using a calcium assay (QuantiChrom; BioAssay Systems).

Protein adsorption onto different materials was assessed by immersing 75 µL of ceramics in 1 mL of medium (containing 10% FBS, as described below) at 37 °C. After the indicated time points, the adsorbed proteins were lysed from the ceramics constructs with 150 µL RIPA (radio-immunoprecipitation assay) buffer with phosphatase and protease inhibitors. The ceramic particles were crushed and sonicated on ice, after which they were centrifuged for 10 min at 12 000 *g* at 4 °C. Total protein content of the supernatant was determined using a protein assay (BCA, Pierce).

5.3. In Vivo Characterization of Ectopic Bone Forming Capacity

Surgery was performed on six adult dogs (mongrel, male, 10–15 kg, 1–2 years old) with the permission of the local animal care committee (Animal Centre, Sichuan University, Chengdu, China). All surgeries were conducted under general anesthesia by abdominal injection of sodium pentobarbital (30 mg kg^{-1} body weight). After shaving and sterilizing with iodine, a longitudinal skin incision and a median fascial incision were made, and the paraspinal muscles were exposed. Muscle pouches with length larger than 2 cm were made along the paraspinal muscle with blunt separation. Ceramic particles (1 mm) of HAn, HAi, BCPn, BCPi and TCP, or dense cylinders with cut gaps of TCPa and TCPb were loaded in individual muscle pouches. After the implants were sealed in the muscle pouches with silk sutures, the skin was suture closed. Following surgery, the animals were intramuscularly administered buprenorphine (0.1 mg per animal) for two days to relieve pain, and penicillin (40 mg kg^{-1}) for three days to prevent infection. The animals were allowed full weight-bearing and received a normal diet. After 12 weeks, the animals were sacrificed with an abdominal injection of sodium pentobarbital. Implants were harvested with surrounding tissue, trimmed, fixed in 4% formaldehyde, dehydrated with a gradient ethanol scale and embedded in PMMA. Non-decalcified sections were made using a diamond saw, stained with 1% methylene blue and 0.3% basic fuchsin solutions for light microscopy.

5.4. Replication of Surface Microtopography of Ceramics in Polystyrene

To replicate the topographical structure of ceramics in polystyrene substrates, two TCP ceramic discs were first imprinted in an intermediate mold of cyclic olefin copolymer (COC) (T_g = 140 °C, 100 µm thickness). A hot embossing nanoimprint lithography machine (NIL 6", Obducat, Malmö, Sweden) was used at 160 °C and 50 bars pressure for 300 s, followed by cooling and demolding at 60 °C. Thereafter, the intermediate mold was incubated in 1 M HCl for 1 h in order to remove the ceramic layer without influencing the topographical features. The COC intermediate molds were treated with oxygen plasma (50 sccm O_2, 50 W, 75 mTOR, 30 s) prior to coating with fluorooctatrichlorosilane (FOTS). Finally, they were used to replicate the topographical features in polystyrene thin films (oriented PS, Polyflex clear grade, 75 µm thickness, Sidaplax). Again, hot embossing was used at 115 °C and 50 bar pressure for 300 s, followed by cooling and demolding at 60 °C. After imprinting, the polystyrene films replicating the topography of the ceramic discs were treated with oxygen plasma and sterilized in ethanol. Characterization of the replication was done by visual observation following SEM imaging.

5.5. Cell Culture

The human osteosarcoma cell line MG-63 was expanded in medium consisting of α-minimal essential medium supplemented 10% fetal bovine serum, 0.2×10^{-3} M ascorbic acid, 2×10^{-3} M L-glutamine, 100 U mL^{-1} penicillin, and 100 µg mL^{-1} streptomycin. To investigate the effect of the ceramics, 200 000 cells in 100 µL of medium were seeded per 150 µL of particles pre-wetted with medium and allowed to attach for 4 h before adding additional medium. The cell-material constructs were cultured for 48 h or 7 days. As a reference, cells were seeded at low density (5 000 cells per cm^2) and at high density (25 000 cells per cm^2) on tissue culture polystyrene.

5.6. Transcriptional Profiling

5.6.1. RNA Isolation

After cell culture on the different materials, total RNA was isolated using the Nucleospin RNA isolation kit (Macherey–Nagel). Then, from 275 ng of RNA, cRNA was synthesized using the Illumina TotalPrep RNA amplification kit, and both RNA and cRNA quality were verified on a Bioanalyzer 2100 (Agilent).

5.6.2. Gene Expression Profiling

Microarrays were performed using Illumina HT-12 v4 expression Beadchips. Briefly, 750 ng of cRNA was hybridized on the array overnight, after which the array was washed and blocked. Then, by addition of streptavidin Cy-3, a fluorescent signal was developed. Arrays were scanned on an Illumina Beadarray reader and raw intensity values were background corrected in BeadStudio (Illumina). Further data processing and statistical testing were performed using R and Bioconductor statistical software (reference). Graphical visualization of the data was obtained using GeneSpring software (Agilent Technologies and Strand Life Sciences). The probe-level raw intensity values were quantile normalized and transformed using variance stabilization (VSN). A linear modeling approach with empirical Bayesian methods, as implemented in Limma package,[57] was applied for differential expression analysis of the resulting probe-level expression values. *P*-values were corrected for multiple testing using the Benjamini and Hochberg method.[58] Genes were considered differentially expressed when a corrected *p*-value below 0.05 was reached.

5.6.3. Pathway and Network Analysis

Pathway over-representation analysis was performed using the webtool ConsensusPathDB (CPDB), which provides a comprehensive pathway analysis covering most public resources for interactions.[59] Over-representation analysis was performed on a set of differentially expressed genes and a background list containing all measured genes was used to improve the statistical evaluation of the pathways. Pathways with a false discovery rate-corrected *p*-value <0.05 were considered significant.

Network analysis was carried out in two steps. CPDB contains an induced network module which uses the interactions described in all the public resources to build a network based on a list of input genes. At first a network was generated on the same list of differentially expressed genes as used for pathway analysis using a z-score threshold of 18. Only binary protein interactions of low, medium, and high confidence were selected and intermediate genes were allowed to be added to the network in order to improve inter-gene connectivity. The resulting network was subsequently imported into CytoScape and the plugin CyTargetLinker was used to extend the CPDB network by adding transcription factors from the transcription factor target databases ENCODE (ENCyclopedia Of DNA Elements, proximal targets) and TFe (Transcription Factor encyclopedia).[60–63] ENCODE is based on a screening of ChIP-seq datasets while TFe is a smaller scale manual literature curation project containing 42 351 and 1531 human transcription factor target interactions respectively. The node degree distribution of the networks was analyzed using the built-in network analyzer option.

5.7. Validation of Datasets

The genes from the above experiment were independently validated in three other datasets. Firstly, a dataset published by Barradas et al.[32] was used. Specifically, donor-derived human mesenchymal stem cells (hMSC) were cultured on HAn and TCP (the same materials as in this study) in medium (same composition as described above) supplemented with 10 nM dexamethasone for various time points including 48 h. The second and third dataset used for validation of the identified genes included the same HAn and TCP ceramic particles on which an immortalized donor derived human mesenchymal stem cell line (iMSC) and MG-63 were cultured (in medium with the same composition) for 48 h.[41]

5.8. Quantitative Polymerase Chain Reaction

In order to investigate the regulation of gene expression, cDNA was prepared from RNA according to the manufacturer's instructions (BioRad, USA). Quantitative RT-PCR was performed in a 20 µL volume with 0.01 nmol of forward and reverse primers. Thermocycling was performed at 60 °C for 15 s and 72 °C for 15 s for 35 cycles. β-2-Microglobulin (*β2M*) was used as a housekeeping gene and relative expression was determined using the ΔΔCT method. Primer sequences are provided in Table S in the Supporting Information.

5.9. Hyaluronic Acid Quantification

For the quantification of hyaluronic acid, 100 000 MG-63 cells in 50 µL of medium were seeded per 75 µL of particles and cultured in phenol-free α-MEM with the same medium components as mentioned above.

5.9.1. ELISA

The hyaluronic acid content in the extracellular matrix and cells adhering to the materials was quantified using the Hyaluronan Quantikine ELISA kit (R&D systems). Cell lysates, obtained by incubation with Cell Lysis Buffer 2 (R&D Systems) were loaded onto the ELISA plate and processed following the manufacturer's instructions.

5.9.2. Hyaluronic Acid Size Analysis by Agarose Gel Electrophoresis

Cells cultured on the ceramic particles were washed once with PBS and subsequently subjected to proteinase K digestion for 4 h at 60 °C, vortexing every 30 min. The ceramics were removed by centrifugation and the supernatant was precipitated in 4 volumes of pre-chilled ethanol and incubated overnight at –20 °C. The next day, the samples were pelleted by centrifugation at 14 000×*g* for 10 min at RT. The pellet was washed using 4 volumes of pre-chilled 75% ethanol while vortexing. After a second centrifugation step, the supernatant was removed and the pellet air-dried for 20 min at RT. The dried pellet was resuspended in 100 µL of 100×10^{-3} M ammonium acetate. Proteinase K was inactivated by incubating the samples at 100 °C for 5 min and then chilled on ice. Thereafter, nucleic acids were digested by incubation overnight with DNAse and RNAse A at 37 °C. The enzymes were inactivated in a boiling water bath for 5 min after which 400 µL of ethanol were added and incubated overnight at –20 °C. The samples were pelleted as before and washed with 1 mL of cold 75% ethanol. After centrifugation and removal of the supernatant, the pellets were air-dried and resuspended in 20 µL of ammonium acetate (100×10^{-3} M at pH 7). Half of each sample was digested with 1 µL of hyaluronidase (from *Streptomyces hyalurolyticus*, Sigma). The samples and a low-molecular-weight hyaluronic acid reference (15–30 kDa) were subsequently loaded on a 1% agarose gel and the resulting bands were visualized after staining with Stains-All (Sigma).

5.10. Statistics

Experiments carried out in duplicate or triplicate (as indicated in the figure legends) are defined respectively as two or three independent samples that were treated, isolated and analyzed separately. All experiments are presented as the mean ± standard deviation. Assays were analyzed using one or two way analysis of variance (ANOVA) with Bonferroni's multiple comparison test, post-hoc Tukey test or Dunnett's test, comparing the groups of interest. Statistics used during bioinformatics characterization are explained in detail in the respective subsection on gene expression profiling.

Supporting Information

Supporting Information is available from the Wiley Online Library or from the author.

Acknowledgements

The authors declare no conflict of interest. This research forms part of the Project P2.04 BONE-IP of the research program of the BioMedical Materials (BMM) Institute, co-funded by the Dutch Ministry of Economic Affairs. The authors would also like to acknowledge the financial support of the Dutch province of Limburg in the LINK ("Limburg INvesteert in haar Kenniseconomie") knowledge economy project.

Received: June 21, 2016
Revised: October 7, 2016
Published online: December 19, 2016

[1] A. D. Celiz, J. G. Smith, R. Langer, D. G. Anderson, D. A. Winkler, D. A. Barrett, M. C. Davies, L. E. Young, C. Denning, M. R. Alexander, *Nat. Mater.* **2014**, *13*, 570.
[2] S. W. Cranford, J. de Boer, C. van Blitterswijk, M. J. Buehler, *Adv. Mater.* **2013**, *25*, 802.
[3] *Materiomics – High-Throughput Screening of Biomaterial Properties*, (Eds: J. De Boer, C. A. van Blitterswijk), Cambridge University Press, New York **2013**.
[4] M. P. Lutolf, P. M. Gilbert, H. M. Blau, *Nature* **2009**, *462*, 433.
[5] M. J. Biggs, R. G. Richards, M. J. Dalby, *Nanomedicine* **2010**, *6*, 619.
[6] S. Samavedi, A. R. Whittington, A. S. Goldstein, *Acta Biomater.* **2013**, *9*, 8037.
[7] D. Sen, M. J. Buehler, *Sci. Rep.* **2011**, *1*, 35.
[8] H. V. Unadkat, M. Hulsman, K. Cornelissen, B. J. Papenburg, R. K. Truckenmuller, A. E. Carpenter, M. Wessling, G. F. Post, M. Uetz,

M. J. Reinders, D. Stamatialis, C. A. van Blitterswijk, J. de Boer, *Proc. Natl. Acad. Sci. USA* **2011**, *108*, 16565.
[9] L. H. Nguyen, N. Annabi, M. Nikkhah, H. Bae, L. Binan, S. Park, Y. Kang, Y. Yang, A. Khademhosseini, *Tissue Eng., Part B* **2012**, *18*, 363.
[10] D. Pastorino, C. Canal, M. P. Ginebra, *Acta Biomater.* **2015**, *28*, 205.
[11] A. M. Barradas, H. Yuan, C. A. van Blitterswijk, P. Habibovic, *Eur. Cells Mater.* **2011**, *21*, 407.
[12] E. A. Vogler, *Adv. Colloid Interface Sci.* **1998**, *74*, 69.
[13] N. R. Blumenthal, O. Hermanson, B. Heimrich, V. P. Shastri, *Proc. Natl. Acad. Sci. USA* **2014**, *111*, 16124.
[14] A. J. Engler, S. Sen, H. L. Sweeney, D. E. Discher, *Cell* **2006**, *126*, 677.
[15] A. L. Gamblin, M. A. Brennan, A. Renaud, H. Yagita, F. Lezot, D. Heymann, V. Trichet, P. Layrolle, *Biomaterials* **2014**, *35*, 9660.
[16] J. Kohn, W. J. Welsh, D. Knight, *Biomaterials* **2007**, *28*, 4171.
[17] E. P. Magennis, A. L. Hook, M. C. Davies, C. Alexander, P. Williams, M. R. Alexander, *Acta Biomater.* **2016**, *34*, 84.
[18] R. McBeath, D. M. Pirone, C. M. Nelson, K. Bhadriraju, C. S. Chen, *Dev. Cell* **2004**, *6*, 483.
[19] Y. Mei, K. Saha, S. R. Bogatyrev, J. Yang, A. L. Hook, Z. I. Kalcioglu, S. W. Cho, M. Mitalipova, N. Pyzocha, F. Rojas, K. J. Van Vliet, M. C. Davies, M. R. Alexander, R. Langer, R. Jaenisch, D. G. Anderson, *Nat. Mater.* **2010**, *9*, 768.
[20] F. M. Watt, P. W. Jordan, C. H. O'Neill, *Proc. Natl. Acad. Sci. USA* **1988**, *85*, 5576.
[21] W. Habraken, P. Habibovic, M. Epple, M. Bohner, *Mater. Today* **2016**, *19*, 69.
[22] U. Ripamonti, J. Crooks, L. Khoali, L. Roden, *Biomaterials* **2009**, *30*, 1428.
[23] G. D. Winter, B. J. Simpson, *Nature* **1969**, *223*, 88.
[24] H. Yuan, K. Kurashina, J. D. de Bruijn, Y. Li, K. de Groot, X. Zhang, *Biomaterials* **1999**, *20*, 1799.
[25] A. M. Barradas, H. A. Fernandes, N. Groen, Y. C. Chai, J. Schrooten, J. van de Peppel, J. P. van Leeuwen, C. A. van Blitterswijk, J. de Boer, *Biomaterials* **2012**, *33*, 3205.
[26] Y. C. Chai, A. Carlier, J. Bolander, S. J. Roberts, L. Geris, J. Schrooten, H. Van Oosterwyck, F. P. Luyten, *Acta Biomater.* **2012**, *8*, 3876.
[27] O. Nakade, K. Takahashi, T. Takuma, T. Aoki, T. Kaku, *J. Bone Miner. Metab.* **2001**, *19*, 13.
[28] M. J. Dalby, N. Gadegaard, R. Tare, A. Andar, M. O. Riehle, P. Herzyk, C. D. Wilkinson, R. O. Oreffo, *Nat. Mater.* **2007**, *6*, 997.
[29] J. Wang, H. Zhang, X. Zhu, H. Fan, Y. Fan, X. Zhang, *J. Biomed. Mater. Res., Part B* **2013**, *101*, 1069.
[30] J. Wang, Y. Chen, X. Zhu, T. Yuan, Y. Tan, Y. Fan, X. Zhang, *J. Biomed. Mater. Res., Part A* **2014**, *102*, 4234.
[31] X. Li, H. Liu, X. Niu, Y. Fan, Q. Feng, F. Z. Cui, F. Watari, *J. Biomed. Mater Res., Part B* **2011**, *97*, 10.
[32] A. M. Barradas, V. Monticone, M. Hulsman, C. Danoux, H. Fernandes, Z. Tahmasebi Birgani, F. Barrere-de Groot, H. Yuan, M. Reinders, P. Habibovic, C. van Blitterswijk, J. de Boer, *Integr. Biol.* **2013**, *5*, 920.
[33] J. Zhang, X. Luo, D. Barbieri, A. M. Barradas, J. D. de Bruijn, C. A. van Blitterswijk, H. Yuan, *Acta Biomater.* **2014**, *10*, 3254.
[34] C. B. Danoux, D. Barbieri, H. Yuan, J. D. de Bruijn, C. A. van Blitterswijk, P. Habibovic, *Biomatter* **2014**, *4*, e27664.
[35] H. Yuan, H. Fernandes, P. Habibovic, J. de Boer, A. M. Barradas, A. de Ruiter, W. R. Walsh, C. A. van Blitterswijk, J. D. de Bruijn, *Proc. Natl. Acad. Sci. USA* **2010**, *107*, 13614.
[36] A. Bolomsky, H. Ludwig, N. Zojer, *Blood* **2013**, *122*, 5363.
[37] A. Moenning, R. Jager, A. Egert, W. Kress, E. Wardelmann, H. Schorle, *Mol. Cell. Biol.* **2009**, *29*, 881.
[38] A. Raouf, A. Seth, *Oncogene* **2000**, *19*, 6455.
[39] L. Fan, J. Li, Z. Yu, X. Dang, K. Wang, *BioMed. Res. Int.* **2014**, *2014*, 239356.
[40] M. Brunner, P. Jurdic, J. P. Tuckerman, M. R. Block, D. Bouvard, *Int. Rev. Cell Mol. Biol.* **2013**, *305*, 1.
[41] N. Groen, J. van de Peppel, H. Yuan, J. P. van Leeuwen, C. A. van Blitterswijk, J. de Boer, *Biomaterials* **2013**, *34*, 5552.
[42] Y. C. Chai, S. J. Roberts, J. Schrooten, F. P. Luyten, *Tissue Eng., Part A* **2011**, *17*, 1083.
[43] R. Olivares-Navarrete, P. Raz, G. Zhao, J. Chen, M. Wieland, D. L. Cochran, R. A. Chaudhri, A. Ornoy, B. D. Boyan, Z. Schwartz, *Proc. Natl. Acad. Sci. USA* **2008**, *105*, 15767.
[44] Y. R. Shih, Y. Hwang, A. Phadke, H. Kang, N. S. Hwang, E. J. Caro, S. Nguyen, M. Siu, E. A. Theodorakis, N. C. Gianneschi, K. S. Vecchio, S. Chien, O. K. Lee, S. Varghese, *Proc. Natl. Acad. Sci. USA* **2014**, *111*, 990.
[45] C. Wan, S. R. Gilbert, Y. Wang, X. Cao, X. Shen, G. Ramaswamy, K. A. Jacobsen, Z. S. Alaql, A. W. Eberhardt, L. C. Gerstenfeld, T. A. Einhorn, L. Deng, T. L. Clemens, *Proc. Natl. Acad. Sci. USA* **2008**, *105*, 686.
[46] D. S. Bramono, S. Murali, B. Rai, L. Ling, W. T. Poh, Z. X. Lim, G. S. Stein, V. Nurcombe, A. J. van Wijnen, S. M. Cool, *Bone* **2012**, *50*, 954.
[47] Y. J. Jung, A. S. Lee, T. Nguyen-Thanh, K. P. Kang, S. Lee, K. Y. Jang, M. K. Kim, S. H. Kim, S. K. Park, W. Kim, *Biochem. Biophys. Res. Commun.* **2015**, *466*, 339.
[48] A. C. Midgley, L. Duggal, R. Jenkins, V. Hascall, R. Steadman, A. O. Phillips, S. Meran, *J. Biol. Chem.* **2015**, *290*, 11218.
[49] S. Kale, S. Biermann, C. Edwards, C. Tarnowski, M. Morris, M. W. Long, *Nat. Biotechnol.* **2000**, *18*, 954.
[50] S. L. Hyzy, R. Olivares-Navarrete, Z. Schwartz, B. D. Boyan, *J. Cell. Biochem.* **2012**, *113*, 3236.
[51] J. P. van Leeuwen, J. C. Birkenhager, G. C. van den Bemd, H. A. Pols, *Biochim. Biophys. Acta* **1996**, *1312*, 54.
[52] N. L. Davison, J. Su, H. Yuan, J. J. van den Beucken, J. D. de Bruijn, F. Barrere-de Groot, *Eur. Cells Mater.* **2015**, *29*, 314.
[53] C. M. Champagne, J. Takebe, S. Offenbacher, L. F. Cooper, *Bone* **2002**, *30*, 26.
[54] A. M. Barradas, H. Yuan, J. van der Stok, B. Le Quang, H. Fernandes, A. Chaterjea, M. C. Hogenes, K. Shultz, L. R. Donahue, C. van Blitterswijk, J. de Boer, *Biomaterials* **2012**, *33*, 5696.
[55] N. Crosetto, M. Bienko, A. van Oudenaarden, *Nat. Rev. Genet.* **2015**, *16*, 57.
[56] R. Ke, M. Mignardi, A. Pacureanu, J. Svedlund, J. Botling, C. Wahlby, M. Nilsson, *Nat. Methods* **2013**, *10*, 857.
[57] J. M. Wettenhall, G. K. Smyth, *Bioinformatics* **2004**, *20*, 3705.
[58] Y. Benjamini, Y. Hochberg, *J. R. Stat. Soc. B.* **1995**, *57*, 289.
[59] A. Kamburov, U. Stelzl, H. Lehrach, R. Herwig, *Nucleic Acids Res.* **2013**, *41*, D793.
[60] E. P. Consortium, *Science* **2004**, *306*, 636.
[61] M. Kutmon, T. Kelder, P. Mandaviya, C. T. Evelo, S. L. Coort, *PLoS One* **2013**, *8*, e82160.
[62] P. Shannon, A. Markiel, O. Ozier, N. S. Baliga, J. T. Wang, D. Ramage, N. Amin, B. Schwikowski, T. Ideker, *Genome Res.* **2003**, *13*, 2498.
[63] D. Yusuf, S. L. Butland, M. I. Swanson, E. Bolotin, A. Ticoll, W. A. Cheung, X. Y. Zhang, C. T. Dickman, D. L. Fulton, J. S. Lim, J. M. Schnabl, O. H. Ramos, M. Vasseur-Cognet, C. N. de Leeuw, E. M. Simpson, G. U. Ryffel, E. W. Lam, R. Kist, M. S. Wilson, R. Marco-Ferreres, J. J. Brosens, L. L. Beccari, P. Bovolenta, B. A. Benayoun, L. J. Monteiro, H. D. Schwenen, L. Grontved, E. Wederell, S. Mandrup, R. A. Veitia, H. Chakravarthy, P. A. Hoodless, M. M. Mancarelli, B. E. Torbett, A. H. Banham, S. P. Reddy, R. L. Cullum, M. Liedtke, M. P. Tschan, M. Vaz,

A. Rizzino, M. Zannini, S. Frietze, P. J. Farnham, A. Eijkelenboom, P. J. Brown, D. Laperriere, D. Leprince, T. de Cristofaro, K. L. Prince, M. Putker, L. del Peso, G. Camenisch, R. H. Wenger, M. Mikula, M. Rozendaal, S. Mader, J. Ostrowski, S. J. Rhodes, C. Van Rechem, G. Boulay, S. W. Olechnowicz, M. B. Breslin, M. S. Lan, K. K. Nanan, M. Wegner, J. Hou, R. D. Mullen, S. C. Colvin, P. J. Noy, C. F. Webb, M. E. Witek, S. Ferrell, J. M. Daniel, J. Park, S. A. Waldman, D. J. Peet, M. Taggart, P. S. Jayaraman, J. J. Karrich, B. Blom, F. Vesuna, H. O'Geen, Y. Sun, R. M. Gronostajski, M. W. Woodcroft, M. R. Hough, E. Chen, G. N. Europe-Finner, M. Karolczak-Bayatti, J. Bailey, O. Hankinson, V. Raman, D. P. LeBrun, S. Biswal, C. J. Harvey, J. P. DeBruyne, J. B. Hogenesch, R. F. Hevner, C. Heligon, X. M. Luo, M. C. Blank, K. J. Millen, D. S. Sharlin, D. Forrest, K. Dahlman-Wright, C. Zhao, Y. Mishima, S. Sinha, R. Chakrabarti, E. Portales-Casamar, F. M. Sladek, P. H. Bradley, W. W. Wasserman, *Genome Biol.* **2012**, *13*, R24.